

## Integer versus half-integer spin on an approximate honeycomb lattice

V. J. Stewart<sup>1,2</sup>, J. R. Chamorro<sup>1,2</sup>, and T. M. McQueen<sup>1,2,3,\*</sup>

<sup>1</sup>*Department of Chemistry, The Johns Hopkins University, Baltimore, Maryland 21218, USA*

<sup>2</sup>*Institute for Quantum Matter, Department of Physics and Astronomy, The Johns Hopkins University, Baltimore, Maryland 21218, USA*

<sup>3</sup>*Department of Materials Science and Engineering, The Johns Hopkins University, Baltimore, Maryland 21218, USA*



(Received 30 March 2021; revised 15 July 2021; accepted 13 August 2021; published 7 September 2021)

Recent interest in honeycomb lattice materials has focused on their potential to host quantum spin liquid (QSL) states. Variations in bond angles and spin allow a range of interesting behaviors on this lattice, from the predicted QSL ground state of the Kitaev model to exotic magnetic orders. Here we report the physical properties of two compounds with rare earths on an approximate honeycomb lattice. The isostructural compounds  $\text{Nd}_2\text{S}_5\text{Sn}$  ( $J = \frac{9}{2}$ ) and  $\text{Pr}_2\text{S}_5\text{Sn}$  ( $J = 4$ ) permit a direct comparison of half-integer versus integer spins on this lattice. We find strikingly different magnetic properties for the two compounds.  $\text{Nd}_2\text{S}_5\text{Sn}$  orders antiferromagnetically at  $T_N \approx 2.5$  K and undergoes several magnetic transitions to other ordered states under applied field.  $\text{Pr}_2\text{S}_5\text{Sn}$  displays no magnetic ordering transition above  $T = 0.41$  K, and may be proximate to a spin liquid state.

DOI: [10.1103/PhysRevMaterials.5.094401](https://doi.org/10.1103/PhysRevMaterials.5.094401)

### I. INTRODUCTION

Honeycomb lattice materials have been of recent interest as quantum spin liquid (QSL) candidates, as they can host magnetically frustrated spin configurations that may have a disordered ground state [1–3]. Much of this interest has arisen due to the Kitaev model, which predicts a quantum spin liquid ground state on a honeycomb lattice with the right magnetic exchange interactions and is exactly solvable for  $S = \frac{1}{2}$  [4]. Candidate materials for this Kitaev spin liquid include  $\alpha\text{-RuCl}_3$  and  $\text{Ir}^{4+}$  honeycomb iridates such as  $\text{Li}_2\text{IrO}_3$  and  $\text{Na}_2\text{IrO}_3$  [3,5]. So far, all of these candidate materials have been found to magnetically order, but the unconventional magnetic orders they adopt suggest that they are adjacent to a QSL state [5–7].

Looking at honeycomb materials beyond the prototypical spin  $\frac{1}{2}$  on an ideally symmetrical lattice is also valuable. The potential of larger spins to allow a QSL state has sometimes been investigated. Higher-spin models cannot be solved exactly and have weaker quantum fluctuations than  $S = \frac{1}{2}$ . Even so, computational studies of  $S = 1$  moments with both Kitaev and Heisenberg interactions predict a spin liquid region of the phase diagram if the Heisenberg/Kitaev exchange ratio is appropriate [8–10].  $A_3\text{Ni}_2\text{XO}_6$  with  $X = \text{Bi}, \text{Sb}$  and  $A = \text{Li}, \text{Na}$  have been suggested as candidate materials [8].

Extensions to the model with a bond-dependent off-diagonal exchange term included along with Kitaev and Heisenberg terms in the Hamiltonian have been proposed to explain the magnetic order seen in  $\text{Na}_2\text{IrO}_3$  [11]. In this material, the absence of global hexagonal or trigonal symmetry allows the Ir-O-Ir bond angles to deviate from  $90^\circ$ . Although this may move the material away from a Kitaev spin liquid

state, it allows study of the relationship between this state and the long-range magnetic orders adopted.

Even in the absence of Kitaev interactions, spins on a honeycomb lattice can display a range of exotic magnetic states [12,13]. Furthermore, recent studies have shown proximal spin liquid behaviors in a number of layered rare earth compounds, including  $\text{NaYbX}_2$  ( $X = \text{O}, \text{Se}$ ) and  $\text{YbMgGaO}_4$ , as well as 3D variants including  $\text{Ce}_2\text{Zr}_2\text{O}_7$  and  $\text{Pr}_2\text{Zr}_2\text{O}_7$  [14–17].

Here we present magnetic and thermodynamic characterization of  $\text{Nd}_2\text{S}_5\text{Sn}$  and  $\text{Pr}_2\text{S}_5\text{Sn}$ , two isostructural materials containing an approximate honeycomb lattice of rare earth ions. They allow a direct comparison between integer ( $\text{Pr}^{3+}$ ) and half-integer ( $\text{Nd}^{3+}$ ) spins on this lattice. Strikingly, despite point charge calculations revealing a very similar single ion ground state, different physical properties result. The half-integer spin  $\text{Nd}_2\text{S}_5\text{Sn}$  orders antiferromagnetically at  $T = 2.5$  K, and undergoes a series of transitions under applied field, adopting an intermediate magnetic order between its antiferromagnetic and ferromagnetic states. In integer-spin  $\text{Pr}_2\text{S}_5\text{Sn}$  on the other hand, no magnetic ordering is observed down to 0.41 K. These results add to our understanding of the complex magnetic behavior seen in honeycomb materials.

### II. METHODS

$\text{Nd}_2\text{S}_5\text{Sn}$ ,  $\text{Pr}_2\text{S}_5\text{Sn}$ , and a nonmagnetic analog  $\text{La}_2\text{S}_5\text{Sn}$  were prepared from stoichiometric ratios of the elements. Starting materials were sealed in quartz tubes under  $\approx 0.2$  bar argon gas and heated at 870 K for 4 h. After cooling and regrinding, pellets of the materials in evacuated quartz tubes were heated at a rate of 100 K/h to 1320 K. After 12 h they were cooled to 870 K at a rate of 15 K/h and water quenched. Air-stable gray powders were obtained. Products were checked with x-ray diffraction, and if necessary

\*mcqueen@jhu.edu

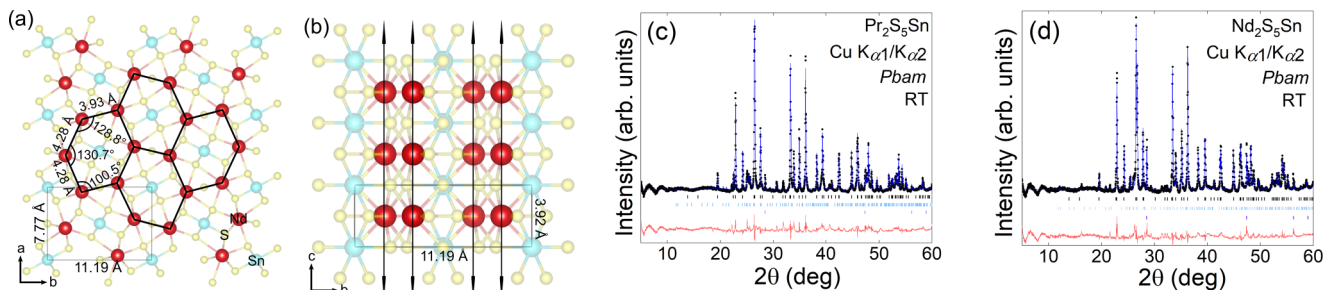


FIG. 1. (a) The structure of  $\text{Nd}_2\text{S}_5\text{Sn}$  in the  $ab$  plane, showing the approximate honeycomb lattice of  $\text{Nd}^{3+}$  ions. Lattice parameters and bond lengths were estimated by refinement of powder x-ray diffraction data in space group  $Pb3m$ . Nd atoms are shown by red spheres, Sn by cyan, and S by yellow. Structural parameters are given to their full precision in Table I, as are the parameters for  $\text{Pr}_2\text{S}_5\text{Sn}$ . (b) The structure in the  $bc$  plane, showing the 1D columns of  $\text{Nd}^{3+}$ . (c) and (d) The PXRD pattern (black circles), refinement (blue line), and differences (red line) for the Pr and Nd compounds. Black, light blue, and purple dashes are the  $hkl$  indices for  $\text{Ln}_2\text{S}_5\text{Sn}$ ,  $\text{Ln}_{10}\text{OS}_{14}$ , and Si, respectively.

additional sulfur was added to the sample and the 1320 K heating cycle was repeated.

Powder x-ray diffraction (PXR) patterns were collected on a laboratory Bruker D8 Focus diffractometer (Cu tube,  $K\alpha_1 = 1.540596 \text{ \AA}$ ,  $K\alpha_2 = 1.544493 \text{ \AA}$ ) with a LynxEye detector. Structural refinements were performed with GSAS-II [18]. Structures were visualized with VESTA [19]. The crystal field splitting for a point charge model of  $\text{Nd}^{3+}$  and  $\text{Pr}^{3+}$  was computed using PYCRYSTFIELD [20].

Magnetization data were collected on a Quantum Design Physical Property Measurement System (PPMS) using the ACMS option, and on a Quantum Design Magnetic Property Measurement System (MPMS). Magnetic susceptibility was approximated as magnetization divided by the applied magnetic field ( $\chi \approx M/H$ ). Heat capacity data were collected on the PPMS using the semiadiabatic method and a 1% temperature rise. For  $\text{Nd}_2\text{S}_5\text{Sn}$ , data from  $T = 0.12\text{--}3.8 \text{ K}$  were collected using a dilution refrigerator. The heat capacity of  $\text{Nd}_2\text{S}_5\text{Sn}$  from  $T = 2\text{--}10 \text{ K}$  was additionally measured using a long-pulse method with 30% temperature rise and analyzed using the LONGPULSEHC software package [21].

### III. RESULTS

#### A. Structure

Both compounds were refined in the space group  $Pb3m$ , consistent with the literature. The structural parameters obtained were also consistent with previous reports [22,23]. Refinement indicated a small  $\text{Ln}_{10}\text{OS}_{14}$  ( $\text{Ln} = \text{Nd}, \text{Pr}$ ) impurity in each compound (estimated weight fraction  $\approx 3\%$  in both compounds). These most likely originate from oxide impurities in the starting materials, and are expected to have minimal effect on the magnetic properties due to their small weight percentage.

The  $\text{Ln}^{3+}$  rare earth ions of  $\text{Pr}_2\text{S}_5\text{Sn}$  form an approximate honeycomb lattice in the  $ab$  plane. Each hexagon of  $\text{Ln}^{3+}$  is skewed away from equilateral, as shown in Fig. 1(a). Along the  $c$  direction, the  $\text{Ln}^{3+}$  ions align to form a column (Table I). Each rare earth is coordinated by nine sulfur atoms, while tin and sulfur are, respectively, octahedrally and tetrahedrally coordinated. This structure may allow  $\text{Ln}_2\text{S}_5\text{Sn}$  to behave as a pseudo-two-dimensional crystal, with each column (a 1D chain) functioning as a single unit for magnetic exchange. In both compounds, the distances between nearest-neighbor

$\text{Ln}^{3+}$  within the planes and along the columns are similar, ranging from  $\approx 3.9$  to  $4.3 \text{ \AA}$  [Fig. 1(a)]. All  $\text{Ln}^{3+}$  atoms are connected via sulfur bonds, and the presence of this bonding between layers makes the stacking fault disorder present in some layered honeycomb materials unlikely here.

#### B. Magnetization

Magnetization versus temperature measurements [ $M(T)$ ] show a clear antiferromagnetic (AFM) phase transition for  $\text{Nd}_2\text{S}_5\text{Sn}$  at  $T_N = 2.6 \text{ K}$ , while  $\text{Pr}_2\text{S}_5\text{Sn}$  appears paramagnetic down to  $T = 0.41 \text{ K}$  (Fig. 2). Parameters obtained from Curie-Weiss fits for each compound are given in Table II. Fits were performed over the range  $T = 30\text{--}300 \text{ K}$ , as well as over a lower temperature range ( $3\text{--}30 \text{ K}$  for  $\text{Nd}_2\text{S}_5\text{Sn}$  and  $2\text{--}30 \text{ K}$  for  $\text{Pr}_2\text{S}_5\text{Sn}$ ) to avoid excited crystal fields. In all cases, best fit was achieved with no temperature-independent contribution ( $\chi_0 = 0$ ). The room temperature susceptibility of the nonmagnetic analog  $\text{La}_2\text{S}_5\text{Sn}$  was  $\chi = -2.06 \times 10^{-4} \text{ emu K (Oe mol Ln}^{3+})^{-1}$ . By comparison to the literature diamagnetic susceptibility of  $\text{La}^{3+}$  [ $\chi_D = -2 \times 10^{-5} \text{ emu K (Oe mol Ln}^{3+})^{-1}$ ], this value is consistent with a negligible  $\chi_0$  [24].

The estimated Weiss temperatures  $\theta_w$  (given in Table II) are negative over both temperature ranges, indicating that antiferromagnetic interactions are dominant. Also for both ranges, the magnitude of  $\theta_w$  is larger for the Nd compound,

TABLE I. Lattice parameters, Ln-Ln distances, and internal angles of the  $\text{Ln}_6$  hexagons determined by Rietveld refinement of PXR data. Distance and angles are given along the perimeter of a hexagon as shown in Fig. 1(a).

	$\text{Nd}_2\text{S}_5\text{Sn}$	$\text{Pr}_2\text{S}_5\text{Sn}$
$a$ ( $\text{\AA}$ )	7.7723(3)	7.7690(3)
$b$ ( $\text{\AA}$ )	11.1942(4)	11.2339(4)
$c$ ( $\text{\AA}$ )	3.9168(1)	3.9510(1)
Ln-Ln distances ( $\text{\AA}$ )	3.9337(1)	3.9384(1)
	4.2758(1)	4.2856(1)
	4.2758(1)	4.2856(1)
Ln-Ln-Ln angles (deg)	128.8285(5)	129.8429(4)
	130.702(3)	130.028(2)
	100.470(2)	100.130(2)

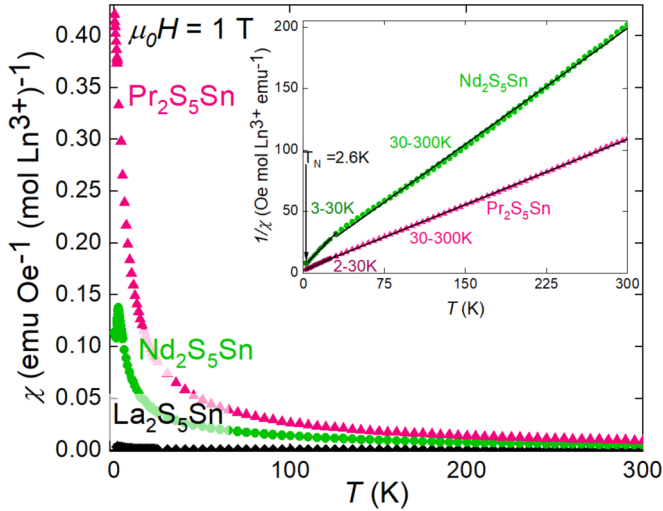


FIG. 2. Magnetization versus temperature for  $\text{Nd}_2\text{S}_5\text{Sn}$  (green circles) and  $\text{Pr}_2\text{S}_5\text{Sn}$  (pink triangles). The inset shows Curie-Weiss fits to high and low temperature regions for each compound. The nonmagnetic analog  $\text{La}_2\text{S}_5\text{Sn}$  (black diamonds) is also included for reference.

meaning that the interaction strength is larger than in the Pr. The effective magnetic moments calculated from the Curie constant are somewhat higher than the free-ion moment for Pr ( $3.58 \mu_B$ ), and lower than the free-ion moment for Nd ( $3.62 \mu_B$ ).

Crystal field splitting computed from the point charge model offer an explanation for the large moment of Pr (Fig. 3).  $\text{Nd}^{3+}$  ( $J = \frac{9}{2}$ ) splits into five Kramers doublets, while  $\text{Pr}^{3+}$  ( $J = 4$ ) splits into nine singlet states. In  $\text{Pr}^{3+}$ , the energy gap between the two lowest states is only  $0.27 \text{ meV}$  ( $\approx 2.6 \text{ K}$ ). Due to this low energy barrier, these states may act as a pseudodoublet, allowing an effective  $J = \frac{1}{2}$  and providing the unpaired spins necessary for the paramagnetic behavior of  $\text{Pr}_2\text{S}_5\text{Sn}$ .

The influence of these crystal field levels means that the higher-temperature Curie-Weiss fits are likely to be unreliable. However, they are included for the sake of comparison. The lower-temperature fits, in which  $p_{\text{eff}} = 4.49(2)$  for Pr and  $p_{\text{eff}} = 2.96(2)$  for Nd, can additionally be compared to the low-temperature moments for the Pr and Nd pyrochlores, which are also magnetically frustrated and have properties significantly influenced by their crystal field states:  $\text{Pr}_2\text{Pb}_2\text{O}_7$  [ $p_{\text{eff}} = 2.53(1) \mu_B$ ],  $\text{Pr}_2\text{Zr}_2\text{O}_7$  [ $p_{\text{eff}} = 2.5(1)$

TABLE II. Parameters obtained from Curie-Weiss analysis of  $\text{Nd}_2\text{S}_5\text{Sn}$  and  $\text{Pr}_2\text{S}_5\text{Sn}$  magnetization data. Low temperature (LT) and high temperature (HT) ranges were fitted separately. The units of the Curie constant  $c$  are  $\text{emu K (Oe mol Ln}^{3+})^{-1}$ .

	Pr LT	Pr HT	Nd LT	Nd HT
Range (K)	2–30	30–300	3–30	30–300
$c$	2.529(4)	2.825(1)	1.093(7)	1.589(3)
$\theta$ (K)	−4.7(1)	−7.3(8)	−5.3(5)	−16(5)
$p_{\text{eff}}$ ( $\mu_B$ )	4.49(2)	4.75(1)	2.96(2)	3.57(1)

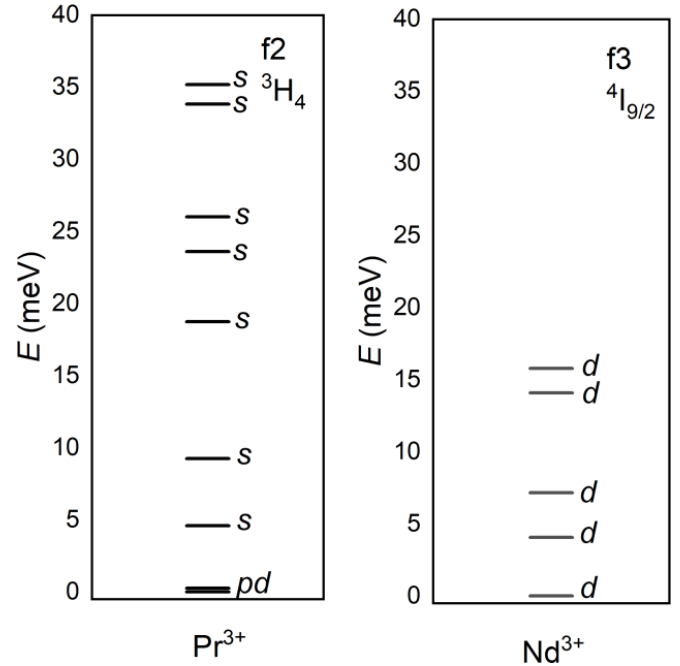


FIG. 3. Computed single-ion crystal field levels for  $\text{Pr}^{3+}$  and  $\text{Nd}^{3+}$ .  $s$  indicates a singlet state,  $d$  a doublet, and  $pd$  a pseudodoublet. The low-energy pseudodoublet of  $\text{Pr}^{3+}$  can explain its paramagnetic behavior.

$\mu_B$ ],  $\text{Pr}_2\text{Sn}_2\text{O}_7$  [ $p_{\text{eff}} = 2.6 \mu_B$ ],  $\text{Nd}_2\text{Pb}_2\text{O}_7$  [ $p_{\text{eff}} = 2.55(7) \mu_B$ ],  $\text{Nd}_2\text{Zr}_2\text{O}_7$  [ $p_{\text{eff}} = 2.543(2) \mu_B$ ], and  $\text{Nd}_2\text{Sn}_2\text{O}_7$  [ $p_{\text{eff}} = 2.63(3) \mu_B$ ] [25–30].

To investigate possible ordering in  $\text{Pr}_2\text{S}_5\text{Sn}$  at  $T < 2 \text{ K}$ ,  $M(T)$  and magnetization versus field [ $M(H)$ ] measurements were performed in a  ${}^3\text{He}$  system (Fig. 4). No evidence of magnetic ordering was found down to  $T = 0.41 \text{ K}$ , either in  $M(T)$  or  $M(H)$  at any field. We thus conclude that  $\text{Pr}_2\text{S}_5\text{Sn}$  remains paramagnetic for  $T > 0.41 \text{ K}$ . The  $M(H)$  curves approach field saturation as expected for a paramagnet at low temperatures, but do not appear to fully saturate in the  $\mu_0 H = 7 \text{ T}$  range measured.

To look more closely at the observed phase transition in  $\text{Nd}_2\text{S}_5\text{Sn}$ ,  $M(H)$  data were collected at temperatures between  $0.45$  and  $6 \text{ K}$  (Fig. 5). Data points with temperature or sample center position values outside of two standard deviations are excluded from the figure. No hysteresis was observed. Derivatives of the  $M(H)$  curves allow clear visualization of the features of this data. At  $T = 3 \text{ K}$  and above, as expected, the  $M$  versus  $H$  curves are smooth and featureless, consistent with the absence of the phase transition at these temperatures.

At lower temperatures, three distinct peaks are present in the derivative: one near  $0.25 \text{ T}$ , one near  $2.2 \text{ T}$ , and one broad peak near  $4 \text{ T}$ . These peaks decrease in intensity and shift to lower field as temperature is raised. By  $2 \text{ K}$ , the  $0.25$  and  $2.2 \text{ T}$  peaks are not discernible, and the derivative curve appears to have one broad hump centered near  $3 \text{ T}$ . This suggests that the loss of antiferromagnetic order with increasing field occurs in three steps, with two intermediate states between full AFM order and full alignment with the applied field. The energy difference between the steps decreases with higher temperature.

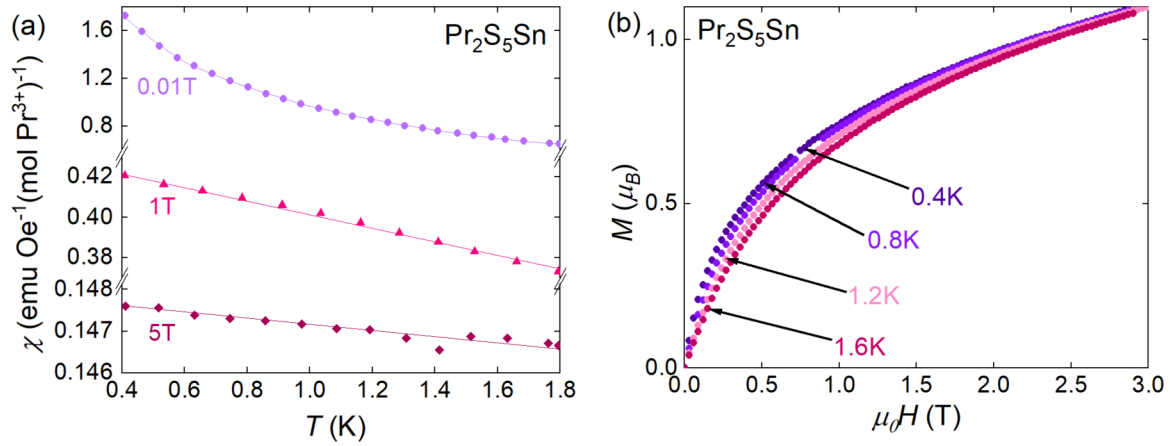


FIG. 4. (a) Magnetization versus temperature for  $\text{Pr}_2\text{S}_5\text{Sn}$ , measured from  $T = 0.4\text{--}1.8$  K in a  $^3\text{He}$  system. Each of the three fields measured is plotted on a different scale to clearly show change versus temperature. Lines are to guide the eye. No ordering transition was observed. (b) Magnetization versus field for  $\text{Pr}_2\text{S}_5\text{Sn}$ .

**C. Heat capacity**

Heat capacity measurements corroborate the magnetization data [Fig. 6(a)]. For  $\text{Pr}_2\text{S}_5\text{Sn}$ , there is a weak divergence of  $C/T$  as  $T \rightarrow 0$ , with no evidence of a phase transition. For  $\text{Nd}_2\text{S}_5\text{Sn}$ , a peak is observed at  $T = 2.4$  K. Poor fitting of temperature curves below  $\approx 6$  K by the semiadiabatic pulse method suggested a first-order phase transition, so a long-pulse technique was used for the low temperature heat capacity. The long-pulse measurements were of larger magnitude near the peak at  $T = 2$  K but were in good agreement with the short-pulse data above the peak temperature, consistent with the phase transition being first order. Additional short-pulse data collected down to  $T = 0.12$  K with a dilution refrigerator is truncated at 1.8 K to avoid the first-order peak.

The phonon heat capacity, estimated from the nonmagnetic analog  $\text{La}_2\text{S}_5\text{Sn}$ , was subtracted to find the magnetic contribution  $C_m$  [Fig. 6(a) inset]. The upturn at low temperature is due to the nuclear specific heat. The magnetic entropy was calculated by integrating  $C_m/T$  [Fig. 6(b)]. For the Nd compound, entropy passes  $\Delta S = R\ln 2$  near 5 K, which is sensible given its doublet ground state. It briefly plateaus, and then

rises to  $\Delta S = R\ln 3$  by 100 K. This is qualitatively consistent but somewhat less than expected from the point charge model, suggesting that the second excited doublet state is somewhat higher in energy than predicted. For Pr, the entropy reaches  $\Delta S = R\ln 2$  around 35 K before plateauing, suggesting that only the two lowest-lying energy levels are accessible. The gradual further increase in entropy up to 50 K is qualitatively consistent with expectations and suggests that the energy gap to the third singlet state is again larger than predicted by the crystal field splitting model. Above  $\approx 100$  K for the Nd compound and  $\approx 50$  K for the Pr, the small magnitude of the magnetic heat capacity compared to the subtracted phonon contribution makes the computed entropy unreliable.

The heat capacity of both compounds was also measured under magnetic field (Fig. 7). For  $\text{Nd}_2\text{S}_5\text{Sn}$ , the  $T = 2.4$  K peak is suppressed with field as expected, since the presence of a large magnetic field disrupts antiferromagnetic ordering. The peak gradually decreases in magnitude from  $\mu_0 H = 0$  to 3 T, and seems to disappear completely between  $\mu_0 H = 3$  and 5 T. This change is visible in the magnetic entropy of these field measurements (Fig. 8), which drops below the

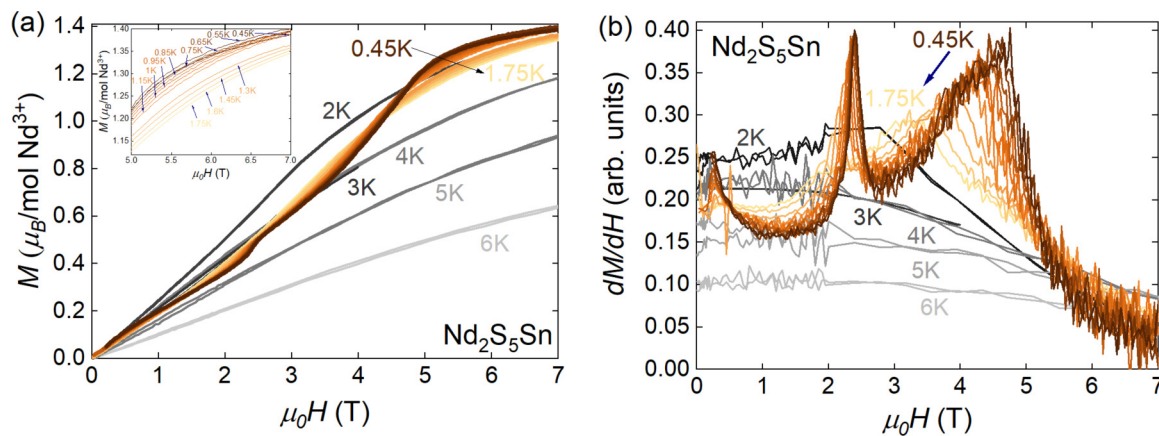


FIG. 5. (a) Magnetization versus field for  $\text{Nd}_2\text{S}_5\text{Sn}$  at temperatures from  $T = 0.45\text{--}6$  K. The inset shows the temperature spacing in the  $\mu_0 H = 5\text{--}7$  T region. No hysteresis was observed in field sweeps. (b) Derivative of  $\text{Nd}_2\text{S}_5\text{Sn}$  magnetization vs field, showing three distinct peaks at temperatures below 2 K.

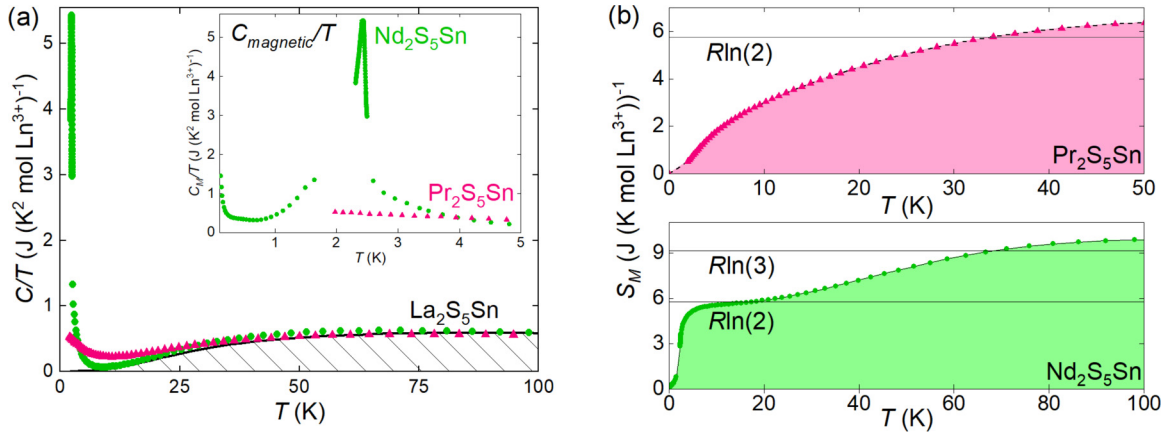


FIG. 6. (a) Heat capacity over temperature ( $C/T$ ) of  $\text{La}_2\text{S}_5\text{Sn}$ ,  $\text{Nd}_2\text{S}_5\text{Sn}$ , and  $\text{Pr}_2\text{S}_5\text{Sn}$ . The inset shows the magnetic heat capacity of  $\text{Nd}_2\text{S}_5\text{Sn}$  and  $\text{Pr}_2\text{S}_5\text{Sn}$ , with the estimated phonon heat capacity subtracted. (b) Magnetic entropy of  $\text{Nd}_2\text{S}_5\text{Sn}$  (top, green) and  $\text{Pr}_2\text{S}_5\text{Sn}$  (bottom, pink), computed by integration of  $C_M/T$ .

$R \ln 2$  plateau at and above  $\mu_0 H = 3$  T, suggesting that some magnetic states are no longer frozen out or that higher energy states have become inaccessible. This change between  $\mu_0 H = 1$  and 3 T may correspond to the sharp peak in  $dM/dH$  near 2.2 T. Additionally, the flattening of the heat capacity peak at 2.4 K with increasing field, and its disappearance by  $\mu_0 H = 5$  T, is in agreement with the broad  $dM/dH$  peak between 3 and 5 T.

#### IV. DISCUSSION

Both our magnetic and thermodynamic measurements make it clear that although they are isostructural, the properties of  $\text{Pr}_2\text{S}_5\text{Sn}$  and  $\text{Nd}_2\text{S}_5\text{Sn}$  are quite distinct. The integer-spin Pr compound is paramagnetic down to at least  $T = 0.41$  K, while the half-integer Nd compound undergoes an antiferromagnetic ordering transition near  $T = 2.5$  K. Besides this most obvious change, we observe that although the two compounds have nearly the same Weiss temperature ( $\theta_w$ ) in Curie-Weiss fits below 30 K, over the higher temperature

range their  $\theta_w$  values differ significantly. The crystal field splitting for a point charge model of  $\text{Nd}^{3+}$  and  $\text{Pr}^{3+}$  helps explain why. The gap between the lowest-lying states (the doublet in Nd and the “pseudodoublet” in Pr) is large compared to the temperature at 30 K. While both ions effectively have a single doublet state primarily populated, the interaction strengths of the spins in this state may be similar. At higher temperatures, where other energy states are accessible, the differences between the two compounds allow the antiferromagnetic exchange in the Nd to become stronger than that of the Pr.

A magnetic phase diagram for  $\text{Nd}_2\text{S}_5\text{Sn}$  can be constructed from the  $M(H)$  and heat capacity under field results (Fig. 9). From the  $M(H)$  data we observe that the loss of the antiferromagnetic phase with field occurs in three stages, with the field distance between these stages shrinking at higher temperatures. The two higher-field transitions merge together by about  $T = 2$  K, shown in the meeting of the phase boundaries in the diagram. The remaining transition occurs at much

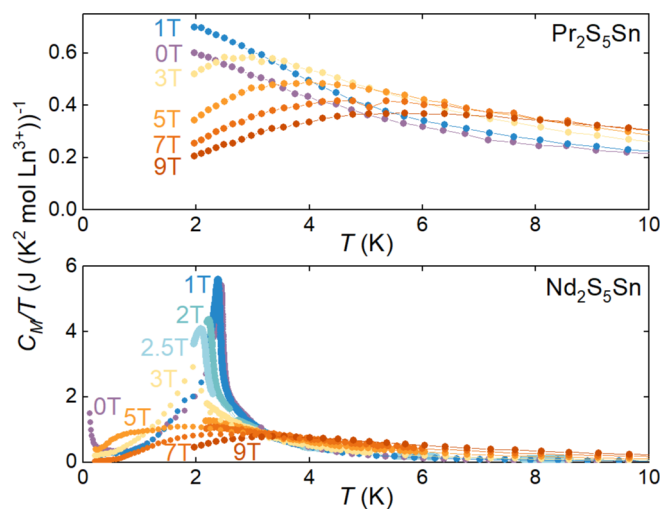


FIG. 7. Magnetic heat capacity (as  $C_M/T$ ) of  $\text{Pr}_2\text{S}_5\text{Sn}$  and  $\text{Nd}_2\text{S}_5\text{Sn}$  under applied magnetic fields. Lines are to guide the eye.

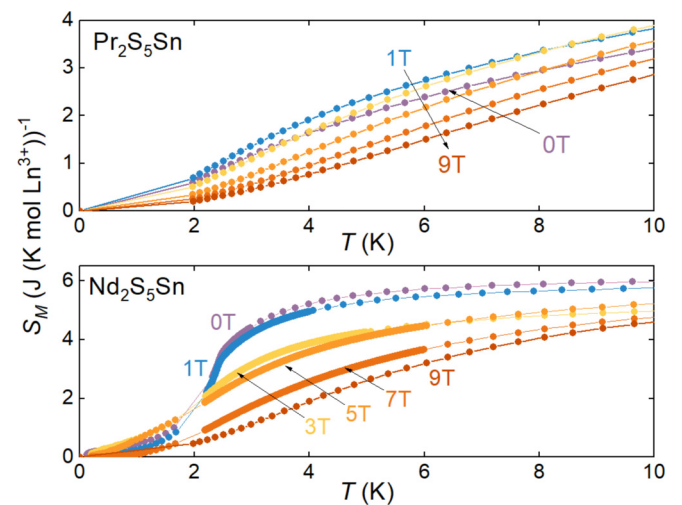


FIG. 8. Magnetic entropy of  $\text{Pr}_2\text{S}_5\text{Sn}$  and  $\text{Nd}_2\text{S}_5\text{Sn}$  under applied magnetic field, computed by integration of  $C_M/T$ . Lines are to guide the eye.

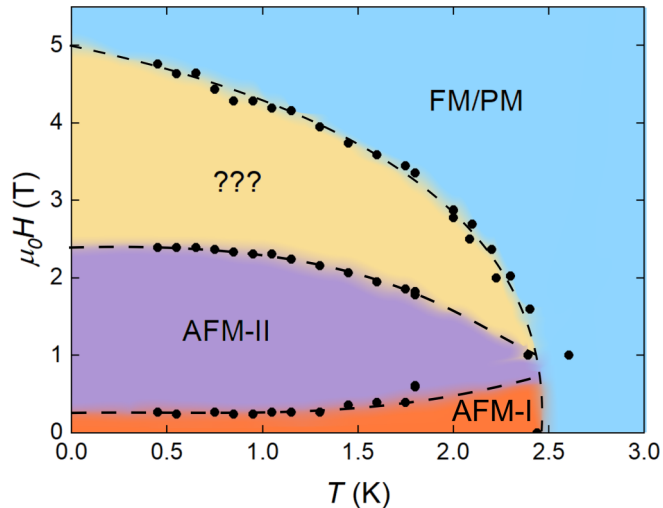


FIG. 9. Magnetic phase diagram of  $\text{Nd}_2\text{S}_5\text{Sn}$ , estimated from magnetization and heat capacity measurements.

lower field ( $\approx 0.25$  T near 1 K), indicating a less energetically difficult change in the magnetic order. Data near  $T = 2.5$  K at low fields is limited, and further study is needed to accurately determine the intersection of the four phases in this region.

How is the magnetic order changing at these metamagnetic transitions? Presumably above the highest field transition, the spins are fully aligned with the applied field, behaving as they would in a ferromagnet. Below this, the specifics of the magnetic order are unknown. The lowest field change may be a spin-flop transition, with spins reorienting to lie parallel to the applied field. In this case, we have one antiferromagnetic ground state and a second intermediate state before all spins align with the field, which is not entirely uncommon in anisotropic antiferromagnets [31–34]. The frustration parameter ( $f = |\frac{\theta_w}{T_N}|$ ) of  $\text{Nd}_2\text{S}_5\text{Sn}$  is  $\approx 2$ , relatively low, so the ground state may be a Néel antiferromagnet. Then at the second transition with field, a subset of the spins may flip along the easy axis, resulting in a magnetic order such as a stripy or zigzag arrangement. Finally, at high enough fields the remaining spins flip to give a ferromagnetic arrangement. Further study is required to understand the specific antiferromagnetic orders present. The easy axis is unknown, as the material has only been measured in powder form, and the large deviation of the lattice from equilateral hexagons may lead to more complicated anisotropic effects.

For  $\text{Pr}_2\text{S}_5\text{Sn}$ , the lack of observed magnetic ordering raises the question of whether it has spin liquid character. Power-law fitting of the field-dependent  $C_m/T$  versus  $T$  did not match the scaling relationship observed in other frustrated spin  $\frac{1}{2}$  materials [35]. Additionally, when performing the Curie-Weiss fits, a linear fit was best achieved with the temperature-independent susceptibility  $\chi_0$  equal to zero, in contrast to many candidate QSL materials [1]. At the same time, the behavior is similar to that observed in QSL candidates based on Pr, such as  $\text{Pr}_2\text{Pb}_2\text{O}_7$ . Further work should clarify the behavior of this material.

## V. CONCLUSION

We have investigated the physical properties of the isostructural approximate honeycomb compounds  $\text{Pr}_2\text{S}_5\text{Sn}$  and  $\text{Nd}_2\text{S}_5\text{Sn}$ , finding that the Pr compound displays no magnetic ordering down to 0.41 K, and that the Nd undergoes antiferromagnetic ordering near  $T = 2.5$  K. These materials may be usefully compared to the lead pyrochlores  $\text{Pr}_2\text{Pb}_2\text{O}_7$  and  $\text{Nd}_2\text{Pb}_2\text{O}_7$ . In these, the Pr material shows no order to 0.4 K but has a spin ice like specific heat anomaly at 1.2 K, which the Nd analog seems to adopt long-range magnetic order at 0.41 K [25]. The similar material  $\text{Pr}_2\text{Zr}_2\text{O}_7$  does not order above 0.2 K and has excitations consistent with a quantum spin system; like  $\text{Pr}_2\text{S}_5\text{Sn}$ , it has a non-Kramers doublet ground state [17,26].  $\text{Pr}_2\text{S}_5\text{Sn}$  lacks order at low temperatures and the minimum frustration parameter  $f = 4.7/0.41$  K = 11 is greater than 10, suggesting the presence of magnetic frustration. Understanding how this frustration occurs on the geometry of this approximate honeycomb is of interest.  $\text{Nd}_2\text{S}_5\text{Sn}$  displays a series of magnetic transitions under applied field and seems to adopt an intermediate magnetic order between its AFM and FM states. Neutron scattering measurements on this compound to determine the magnetic order, and lower-temperature characterization of  $\text{Pr}_2\text{S}_5\text{Sn}$ , would allow us to better understand these materials.

## ACKNOWLEDGMENTS

This work was supported as part of the Institute for Quantum Matter, and Energy Frontier Research Center funded by the U.S. Department of Energy, Office of Science, Office of Basic Energy Sciences, under Award DE-SC0019331. The  $^3\text{He}$  MPMS was funded by the National Science Foundation, Division of Materials Research, Major Research Instrumentation Program, under Award 1828490.

- [1] L. Balents, *Nature (London)* **464**, 199 (2010).
- [2] C. Broholm, R. J. Cava, S. A. Kivelson, D. G. Nocera, M. R. Norman, and T. Senthil, *Science* **367**, eaay0668 (2020).
- [3] J. R. Chamorro, T. M. McQueen, and T. T. Tran, *Chem. Rev.* **121**, 2898 (2021).
- [4] A. Kitaev, *Ann. Phys.* **321**, 2 (2006).
- [5] J. A. Sears, M. Songvilay, K. W. Plumb, J. P. Clancy, Y. Qiu, Y. Zhao, D. Parshall, and Y.-J. Kim, *Phys. Rev. B* **91**, 144420 (2015).

- [6] J. Chaloupka, G. Jackeli, and G. Khaliullin, *Phys. Rev. Lett.* **105**, 027204 (2010).
- [7] Y. Singh, S. Manni, J. Reuther, T. Berlijn, R. Thomale, W. Ku, S. Trebst, and P. Gegenwart, *Phys. Rev. Lett.* **108**, 127203 (2012).
- [8] P. P. Stavropoulos, D. Pereira, and H.-Y. Kee, *Phys. Rev. Lett.* **123**, 037203 (2019).
- [9] X.-Y. Dong and D. N. Sheng, *Phys. Rev. B* **102**, 121102(R) (2020).

- [10] P. H. Y. Li, R. F. Bishop, and C. E. Campbell, *J. Phys.: Conf. Ser.* **702**, 012001 (2016).
- [11] J. G. Rau, E. K.-H. Lee, and H.-Y. Kee, *Phys. Rev. Lett.* **112**, 077204 (2014).
- [12] G. N. Rao, R. Sankar, I. P. Muthuselvam, and F. C. Chou, *J. Magn. Magn. Mater.* **370**, 13 (2014).
- [13] J. W. F. Venderbos, M. Daghofer, J. van den Brink, and S. Kumar, *Phys. Rev. Lett.* **107**, 076405 (2011).
- [14] M. M. Bordelon, C. Liu, L. Posthuma, P. M. Sarte, N. P. Butch, D. M. Pajerowski, A. Banerjee, L. Balents, and S. D. Wilson, *Phys. Rev. B* **101**, 224427 (2020).
- [15] Y. Li, G. Chen, W. Tong, L. Pi, J. Liu, Z. Yang, X. Wang, and Q. Zhang, *Phys. Rev. Lett.* **115**, 167203 (2015).
- [16] J. Gaudet, E. M. Smith, J. Dudemaine, J. Beare, C. R. C. Buhariwalla, N. P. Butch, M. B. Stone, A. I. Kolesnikov, G. Xu, D. R. Yahne, K. A. Ross, C. A. Marjerrison, J. D. Garrett, G. M. Luke, A. D. Bianchi, and B. D. Gaulin, *Phys. Rev. Lett.* **122**, 187201 (2019).
- [17] J.-J. Wen, S. M. Koohpayeh, K. A. Ross, B. A. Trump, T. M. McQueen, K. Kimura, S. Nakatsuji, Y. Qiu, D. M. Pajerowski, J. R. D. Copley, and C. L. Broholm, *Phys. Rev. Lett.* **118**, 107206 (2017).
- [18] B. Toby and R. von Dreele, *J. Appl. Cryst.* **46**, 544 (2013).
- [19] K. Momma and F. Izumi, *J. Appl. Cryst.* **44**, 1272 (2011).
- [20] A. Scheie, *J. Appl. Cryst.* **54**, 356 (2021).
- [21] A. Scheie, *J. Low Temp. Phys.* **193**, 60 (2018).
- [22] P. Jaulmes, *Acta Cryst. Sect. B* **30**, 2283 (1974).
- [23] M. Daszkiewicz, L. Gulay, and V. Shemet, *Acta Cryst. Sect. B* **64**, 172 (2008).
- [24] G. A. Bain and J. F. Berry, *J. Chem. Educ.* **85**, 532 (2008).
- [25] A. M. Hallas, A. M. Arevalo-Lopez, A. Z. Sharma, T. Munsie, J. P. Attfield, C. R. Wiebe, and G. M. Luke, *Phys. Rev. B* **91**, 104417 (2015).
- [26] K. Kimura, S. Nakatsuji, J.-J. Wen, C. Broholm, M. B. Stone, E. Nishibori, and H. Sawa, *Nat. Commun.* **4**, 1934 (2013).
- [27] A. J. Princep, D. Prabhakaran, A. T. Boothroyd, and D. T. Adroja, *Phys. Rev. B* **88**, 104421 (2013).
- [28] K. Matsuhira, Y. Hinatsu, K. Tenya, H. Amitsuka, and T. Sakakibara, *J. Phys. Soc. Jpn.* **71**, 1576 (2002).
- [29] M. Ciomaga Hatnean, C. Decorse, M. R. Lees, O. A. Petrenko, D. S. Keeble, and G. Balakrishnan, *Mater. Res. Express* **1**, 026109 (2014).
- [30] A. Bertin, P. Dalmas de Réotier, B. Fåk, C. Marin, A. Yaouanc, A. Forget, D. Sheptyakov, B. Frick, C. Ritter, A. Amato, C. Baines, and P. J. C. King, *Phys. Rev. B* **92**, 144423 (2015).
- [31] A. Paduan-Filho, M. S. Droiche, and C. C. Becerra, *J. Magn. Magn. Mater.* **54–57**, 699 (1986).
- [32] K. Yamada and J. Kanamori, *Prog. Theor. Phys.* **38**, 541 (1967).
- [33] I. Maartense, I. Yaeger, and B. M. Wanklyn, *Solid State Commun.* **21**, 93 (1977).
- [34] G. F. Tuthill, *J. Phys. C* **14**, 2483 (1981).
- [35] I. Kimchi, J. P. Sheckelton, T. M. McQueen, and P. Lee, *Nat. Commun.* **9**, 4367 (2018).